Intramolecular dephasing and vibrational redistribution in the dispersed fluorescence of ultracold molecules: Application to anthracene

Kaiyu Shan, Yi Jing Yan, and Shaul Mukamel[a)]
Department of Chemistry, University of Rochester, Rochester, New York 14627

(Received 16 February 1987; accepted 23 April 1987)

A reduced description for spectral line shapes in isolated ultracold polyatomic molecules is developed. The vibrational degrees of freedom are partitioned into a system and a bath. The system modes are treated using a Green function eigenstate-free procedure. The bath modes induce intramolecular vibrational redistribution (IVR) and in addition are responsible for intramolecular dephasing resulting from their thermal fluctuations. The effects of the bath are introduced statistically via correlation functions. Application is made to the dispersed fluorescence of ultracold anthracene in a supersonic beam, which shows progression of narrow lines (Raman) and broad redistributed fluorescence. The observed red shift (with respect to the absorption) and line broadening in the emission indicate that the frequencies of the bath modes are on the average 6.4% lower in the electronically excited state compared with the ground state. We further obtain the IVR rates in the high energy region.

I. INTRODUCTION

The calculation of molecular fluorescence and Raman spectra in large anharmonic molecules is one of the fundamental problems in molecular dynamics and spectroscopy.[1–4] Dispersed fluorescence spectra of ultracold polyatomic molecules in supersonic beams[5–11] provide a useful means for studying intramolecular vibrational dynamics. Some general features characterize the variety of molecules studies (e.g., alkylbenzenes, stilbene, pyrazine, ovalene). The absorption (excitation) spectra are discrete, consisting of progressions of a few well-resolved optically active modes. The dispersed fluorescence spectra obtained by excitation to the ground vibronic level (0-0 line) are similar in character to the absorption. However, at higher levels of excitation, the fluorescence typically consists of sharp, well resolved lines superimposed on a broad continuous background. The appearance of the latter complex spectrum is a signature of the molecular anharmonicities. It is therefore clear that supersonic beam line shapes provide a direct probe for intramolecular vibrational dynamics.[6] Parameter and co-workers[3,12] have used chemical timing (i.e., collisional deactivation) to obtain the short-time emission spectra. These experiments demonstrate that the short time emission is narrow, and becomes broad as time evolves. A discussion of these results and their relation to the supersonic beam spectra will be given in Sec. VI.

Zewail and coworkers have recently reported comprehensive picosecond beam studies of anthracene.[9,10] These remarkable experiments demonstrate clearly how spectra which are both time and frequency resolved may carry significant dynamical information even in congested spectral regions with a high density of states, whereby ordinary fluorescence, which is only frequency resolved, may be very complex. These experiments allow us to discuss with confidence the dynamical effects of anharmonics in polyatomic molecules.

The calculation of spectral line shapes (and any other response function) in macroscopic systems is usually made using correlation function methods which are based on a reduced description.[13,14] This is the case for pressure broadening in the gas phase,[15] line shapes in liquids and solid matrices,[16,17] etc. One never attempts to calculate the exact eigenstates of the macroscopic system. The reason is twofold: First, such a calculation is extremely difficult due to the large number of degrees of freedom involved, and second, the experimental broadened line shapes contain highly averaged information and do not reveal properties of individual eigenstates. The calculation of individual eigenstates of macroscopic systems is, therefore, neither feasible nor desirable. The conventional procedure for calculating electronic spectra (absorption, fluorescence and Raman) in isolated molecules requires a complete knowledge of the molecular vibronic eigenstates (level positions and dipole matrix elements). Such an approach is appropriate for small or intermediate size molecules but for large molecules (ten atoms or more) it is impractical. The spectra show intramolecular line broadening in which information on individual eigenstates is highly averaged. This state of affairs is very similar to the behavior of macroscopic systems and it is obvious that methods and techniques developed for the latter may be adopted towards the treatment of intramolecular line broadening of large isolated polyatomic molecules.

We have recently developed a Green function reduced description of spectral line shape of polyatomic molecule in solution.[18–21] Application to fluorescence, Raman, hole burning and nonlinear optical line shapes[22] (e.g., four wave mixing) allowed us to obtain useful information regarding the solvent dynamics and the solvent–solute interaction. In this article we extend that formulation to the spectroscopy of ultracold isolated polyatomic molecules in supersonic beams. The reduced description of intramolecular line shapes[6(a)] is based on partitioning the molecular vibrational degrees of freedom into a few "system" modes, which are strongly coupled to the electronic transition of interest and should be treated explicitly, and the remaining vibra-

[a)] Camille and Henry Dreyfus Teacher–Scholar.

 0021-9606/87/162021-15$02.10

tional modes are treated as a thermal bath using statistical correlation function methods. Once we have identified the system modes and the bath modes, the calculation of the dispersed line shapes of ultracold molecules may be carried out using the formulation developed for line shapes of solvated molecules.[18–21] There are several points which make this calculation quite different from spectra in solution.[6(a)] First, the incident frequency is usually tuned to a narrow, isolated vibronic level in the electronically excited state. This state serves as a *doorway state*, and its contribution is dominant in the emission. This is in contrast to spectroscopy in solution in which many intermediate states are excited simultaneously. This greatly simplifies the theoretical analysis and is the main advantage of supersonic beam spectroscopy. Another fundamental difference exists between the intramolecular bath and a solvent. The solvent has an infinite number of degrees of freedom, and it is normally at a finite temperature. It is, therefore, reasonable to assume that its motions are very weakly correlated with the state of the system. This enables us to use conventional projection operators[23] to eliminate the bath degrees of freedom, assuming that the bath remains in thermal equilibrium throughout the process. For isolated polyatomic moleucles, the situation is very different. The bath is finite and is initially cold ($T=0$ K). As the vibrational relaxation proceeds, the excess vibrational energy is released into the bath. *The state of the bath is, therefore, strongly correlated with the vibronic state of the system.* A formal procedure for overcoming this difficulty was developed previously[6(a),18(c),21] and will be used in this article to construct a microscopic reduced description of dispersed fluorescence in ultracold molecules, which takes the correlated dynamics of the system and the bath into account. In Sec. II we develop the formal expression for the reduced description of dispersed fluorescence. The effect of the bath enters into our final expression [Eq. (13)] through the IVR matrix Γ and the thermal fluctuation correlation function $J_b^d(t)$ which induces dephasing. In Sec. III, we present our model for the IVR matrix and in Sec. IV we develop a microscopic model for the intramolecular dephasing. These results are combined in Sec. V where we present detailed numerical calculations for ultracold anthracene and compare them with experimental supersonic beam spectra.[9,10] Finally in Sec. VI we summarize our results and draw the analogy between the direct and redistributed emission in ultracold molecules, and the Raman and fluorescence spectra observed in condensed phases.

II. DISPERSED FLUORESCENCE OF ULTRACOLD MOLECULES

We consider a polyatomic molecule with two electronic states and N vibrational degrees of freedom. The reduced description is based on dividing the molecular vibrational degrees of freedom into "system modes" denoted Q_S, which are strongly coupled to the electronic transition, and "bath modes" denoted Q_B, which are weakly coupled to the electronic transition. Typically there are few system modes which contribute to the main Franck–Condon progressions in the spectra, and they should be treated explicitly. The number of bath modes is large and they will be treated statistically. The total Hamiltonian of the molecule and the radiation field is

$$H = H_0 + U + H_{\rm int}(t), \tag{1}$$

where

$$H_0 = |g\rangle [H_g(Q_S) + h_g(Q_B)] \langle g| + |e\rangle [H_e(Q_S) + h_e(Q_B) + \omega_{\rm eg}] \langle e|, \tag{1a}$$

$$U = |g\rangle U_g(Q_S,Q_B) \langle g| + |e\rangle U_e(Q_S,Q_B) \langle e|, \tag{1b}$$

and

$$H_{\rm int}(t) = VE(t). \tag{1c}$$

We have partitioned the molecular Hamiltonian into H_0 and U. Here H_g and H_e are Hamiltonians of the system modes in the ground and excited electronic states, $|g\rangle$ and $|e\rangle$, respectively; whereas h_g and h_e are the corresponding bath Hamiltonians. U denotes the interaction between the system and the bath modes, $H_{\rm int}(t)$ represents the radiation–molecule interaction, V is the dipole operator, $E(t)$ is the time dependent external electromagnetic field, and $\omega_{\rm eg}$ is the electronic energy gap (0–0 transition) between the two electronic states. The electronic dipole operator is given by

$$V = \mu(Q_S)[|g\rangle\langle e| + |e\rangle\langle g|], \tag{2}$$

where μ is the electronic transition dipole operator for the system. We shall denote the vibronic eigenstates of the ground state zeroth order system Hamiltonian (H_g) by $|a\rangle$, $|c\rangle$,..., and the eigenstates of H_e by $|b\rangle$, $|d\rangle$,..., etc. The eigenstates of the bath Hamiltonians h_g and h_e will be denoted $|\alpha\rangle$ and $|\beta\rangle$, respectively. The eigenstates of H_0 are direct products of the system and the bath states, i.e.,

$$(H_g + h_g)|\nu,\alpha\rangle = (E_\nu + E_\alpha)|\nu,\alpha\rangle; \quad \nu = a,c,... \tag{3a}$$

and

$$(H_e + h_e)|\nu,\beta\rangle = (E_\nu + E_\beta)|\nu,\beta\rangle; \quad \nu = b,d,... \tag{3b}$$

Here E_ν are the eigenvalues of H_g and H_e, and E_α and E_β are the eigenvalues of h_g and h_e, respectively. We further assume that the dipole operator depends only on the system coordinates and we have,

$$\mu = \sum_{a,b} (\mu_{ab}|a\rangle\langle b| + \mu_{ba}|b\rangle\langle a|), \tag{4}$$

where the summations run over the entire vibronic manifolds in both electronic states. We shall denote the density matrix of the molecule by ρ. It evolves in time following the Liouville equation

$$\frac{d\rho}{dt} = -i[H_0,\rho] - i[U,\rho] - i[H_{\rm int},\rho]. \tag{5a}$$

The anharmonic interaction U between the system and the bath leads to intramolecular vibrational redistribution (IVR). In this article we shall treat the IVR phenomenologically. We, thus, postulate that the effects of U on the system modes can be incorporated by an IVR relaxation matrix Γ which will be specified in Sec. III. We then rewrite the Liouville equation [Eq. (5a)] by eliminating U and adding an IVR matrix, resulting in

$$\frac{d\rho}{dt} = -i[H_0,\rho] + \Gamma\rho - i[H_{\rm int},\rho]. \tag{5b}$$

We shall now introduce Liouville space notation and define the Liouville space operators L and $L_{\rm int}$. When they operate on some dynamic operator B we have

$$LB \equiv [H_0, B] + i\Gamma B, \tag{6a}$$

$$L_{\rm int} B \equiv [H_{\rm int}, B], \tag{6b}$$

Eq. (5b) then assumes the form

$$\frac{d\rho}{dt} = -iL\rho - iL_{\rm int}\rho. \tag{7}$$

We shall further introduce the molecular Liouville space Green's function

$$\mathcal{G}(\tau) \equiv \exp(-iL\tau) \tag{8}$$

and its Fourier transform

$$\mathcal{G}(\omega) \equiv -i\int_0^\infty d\tau \exp(i\omega\tau)\mathcal{G}(\tau) \tag{9a}$$

$$= (\omega - L)^{-1}. \tag{9b}$$

The Liouville space matrix Γ represents vibrational relaxation as well as the radiative decay of the electronically excited state, and it will be specified explicitly in Sec. III.

For a large ultracold molecule in a supersonic beam the molecule is assumed initially at 0 K. Upon interaction with a monochromatic radiation field with frequency ω_L, the molecule can be selectively excited to a single isolated vibronic level, the doorway state $|d,\{0\}\rangle$. The IVR processes result in the population of vibronic states other than $|d,\{0\}\rangle$. Subsequently, an ω_S photon can be emitted either from the doorway state or from the redistributed states $|b,\{\beta\}\rangle$, and the molecule ends up in the $|c,\{\alpha\}\rangle$ state. These two types of emission are observed in a fluorescence emission spectrum as narrow lines and broad components, respectively. The energy level scheme for the fluorescence process is displayed in Fig. 1. The Liouville-space coupling scheme for the fluorescence[14,19,21] is shown in Fig. 2. Here the horizontal bonds represent an interaction V acting from the right, whereas the vertical bonds represent an interaction V acting from the left. There are three independent pathways leading from $|aa\rangle\rangle$ to $|cc\rangle\rangle$ in fourth order in V. (Here $|aa\rangle\rangle$ and $|cc\rangle\rangle$ is the Liouville space notation for $|a\rangle\langle a|$ and $|c\rangle\langle c|$, respectively, see the Appendix). Each of these three pathways has a counterpart, which contributes as a complex conjugate. The steady state rate of emission of ω_S photons is then given by[14,19,21]

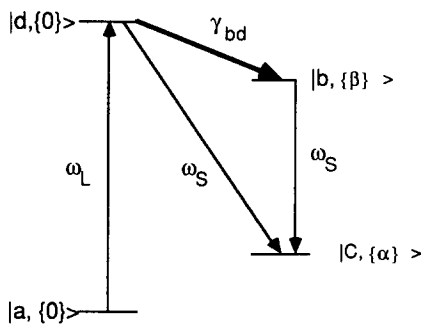

FIG. 1. The energy level scheme for dispersed fluorescence of ultracold anharmonic molecules. ω_L is the incident frequency and ω_S is the emitted frequency. The molecule initially in the $|a,\{0\}\rangle$ absorbs a photon ω_L and goes into the doorway state $|d,\{0\}\rangle$. Direct emission from the doorway state will result in the resonant direct emission whereas IVR relaxation with rate γ_{bd} will populate a state $|b,\{\beta\}\rangle$ in which the bath is hot, and will result in a broad emission.

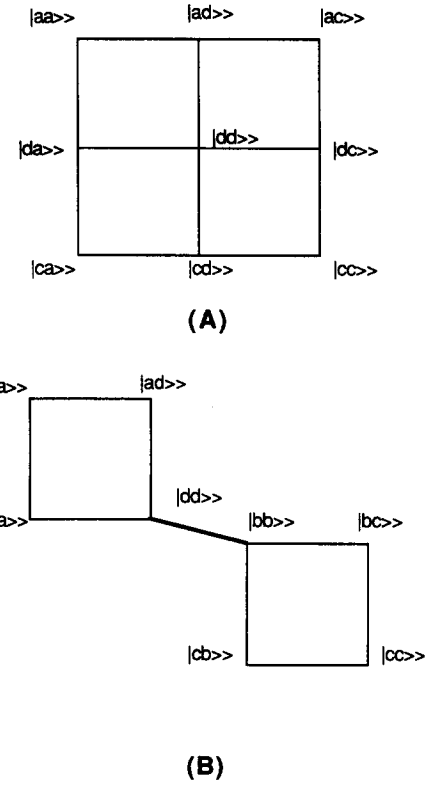

FIG. 2. The Liouville-space coupling scheme for dispersed fluorescence, showing the various pathways which lead from $|aa\rangle\rangle$ to $|cc\rangle\rangle$ (Refs. 14 and 21). The horizontal bonds represent an interaction V acting from the left, whereas the vertical bonds an represent interaction from the right. (A) represents a direct emission from the doorway state. (B) represents the broad emission following IVR from level $|dd\rangle\rangle$ to $|bb\rangle\rangle$.

$$S(\omega_L,\omega_S) = 2\,\mathrm{Re}\sum_c \int_0^\infty dt_1 \int_0^\infty dt_2 \int_0^\infty dt_3 \times [\mathcal{T}_{\rm I} + \mathcal{T}_{\rm II} + \mathcal{T}_{\rm III}] \tag{10a}$$

with

$$\mathcal{T}_{\rm I} = |\mu_{ad}\mu_{dc}|^2 \langle \mathcal{G}_{dc,dc}(t_3)\mathcal{G}_{ac,ac}(t_2)\mathcal{G}_{ad,ad}(t_1)\rangle \times \exp[i\omega_S t_3 - i(\omega_L - \omega_S)t_2 - i\omega_L t_1], \tag{10b}$$

$$\mathcal{T}_{\rm II} = \sum_b |\mu_{ad}\mu_{bc}|^2 \langle \mathcal{G}_{bc,bc}(t_3)\mathcal{G}_{bb,dd}(t_2)\mathcal{G}_{ad,ad}(t_1)\rangle \times \exp[i\omega_S t_3 - i\omega_L t_1], \tag{10c}$$

$$\mathcal{T}_{\rm III} = \sum_b |\mu_{ad}\mu_{bc}|^2 \langle \mathcal{G}_{cb,cb}(t_3)\mathcal{G}_{bb,dd}(t_2)\mathcal{G}_{ad,ad}(t_1)\rangle \times \exp[-i\omega_S t_3 - i\omega_L t_1], \tag{10d}$$

where

$$\mathcal{G}_{\lambda'\delta',\lambda\delta}(t) \equiv \langle\langle \lambda'\delta'|\mathcal{G}(t)|\lambda\delta\rangle\rangle_S = \mathrm{Tr}_S[|\delta'\rangle\langle\lambda'|\mathcal{G}(t)|\lambda\rangle\langle\delta|]. \tag{11}$$

In Eqs. (10) we have assumed that a single doorway state $|d\rangle$ provides the dominant contribution to the emission. In general,[18(c),21] Eqs. (10) will include a summation over $|d\rangle$ as well. Tr_S in Eq. (11) denotes a partial trace over the system degrees of freedom. The angular brackets $\langle ... \rangle$ represent averaging over the bath degrees of freedom, i.e.,

$$\langle \mathcal{G}(t) \rangle = \sum_{\alpha,\alpha'} \mathcal{G}(t)_{\alpha'\alpha',\alpha\alpha}\, \rho_g(\alpha), \tag{12}$$

where $\rho_g(\alpha)$ is the ground state equilibrium density matrix for the bath. In the Appendix we evaluate Eqs. (10) by introducing a factorization approximation which follows the correlated dynamics of the system and the bath. We further assume that the excitation frequency is tuned on resonance with the particular doorway state $|d\rangle$ ($\omega_{ad} + \omega_L = 0$). The emission from this doorway state will be denoted as $S_d(\omega_S)$, and is given by[18(b),21,24]

$$S_d(\omega_S) = -8|\mu_{ad}|^2 \gamma_d^{-2} \sum_b \gamma_b (\Gamma^{-1})_{bb,dd}\, \mathrm{Im}[T_{bb}(\omega_S)]. \tag{13}$$

The T matrix was defined as in Eqs. (6), (7), and (12) of Ref. 18(b), and is given by

$$T_{bb}(\omega) = -i\int_0^\infty d\tau\, T_{bb}(\tau) J_b^d(\tau) \exp(i\omega\tau - \gamma_b|\tau|) \tag{14a}$$

and

$$T_{bb}(\tau) = \langle b|\, \mu \exp[-iH_g(Q_S)t]\, \mu |b\rangle. \tag{14b}$$

$J_b^d(\tau)$ represents the bath line broadening function for emission from the $|b\rangle$ state, following excitation to the doorway state $|d\rangle$:

$$J_b^d(t) = \mathrm{Tr}_B[\exp(-ih_g t)\exp(ih_e t)\rho_b], \tag{14c}$$

ρ_b is the bath density matrix when the system is in the $|b\rangle$ state and the available vibrational energy of the bath is $E_d - E_b$. γ_ν is the inverse lifetime of the state $|\nu\rangle$; $\nu = d,b,...$ and Tr_B represents a partial trace over the bath degrees of freedom.

Equation (13) is the main formal result of this article.[6(a),21] The dispersed fluorescence is given in terms of three basic quantities: $T_{bb}(\tau)$, $J_b^d(t)$, and the Γ matrix. $T_{bb}(\tau)$ contains the Franck–Condon envelope for emission from the state $|b\rangle$ in the absence of the bath. The effects of the bath enter in the other two quantities. $J_b^d(t)$ represents the dephasing effect of the bath. This results from thermal fluctuations in the bath which cause line broadening without affecting the populations of the system states. Im $T_{bb}(\omega_S)$ represents the emission line shape from state $|b\rangle$ broadened by the interaction with the bath.[18(b)] The Γ matrix represents the IVR, i.e., vibrational relaxation which changes the occupation number of the system states. The summation in Eq. (13) runs over the entire excited state manifold including the doorway state $b = d$. For $T_{dd}(\omega_S)$, $J_d^d(\tau) = 1$. The emission is not broadened since the bath is cold. The $b = d$ term, thus, represents a progression of narrow lines from the doorway state. In fact, as is shown in the Appendix, the $b = d$ term is the Raman emission. The emission from $b \neq d$ will be broadened since the bath has now a finite amount of energy. The $b \neq d$ terms are induced by the IVR (off diagonal elements of $\Gamma^{-1}_{bb,dd}$) and they constitute a broad redistributed emission. In the coming sections we shall develop an explicit model which will enable us to calculate Eq. (13).

III. THE INTRAMOLECULAR VIBRATIONAL REDISTRIBUTION MATRIX

When the density of states of the bath modes is sufficiently high, the IVR processes can be described by a rate equation.[6] The IVR rate from level $|b\rangle$ of the system to level $|b'\rangle$ is given by the Fermi Golden rule

$$\Gamma_{b'b',bb} = \frac{2\pi}{\hbar} \sum_{\beta,\beta'} P(\beta) |\langle b',\beta'|U|b,\beta\rangle|^2 \times \delta(\omega_{b'b} - \omega_{\beta'\beta}), \tag{15}$$

where $P(\beta)$ is the population of the bath state $|\beta\rangle$, $\omega_{\nu\mu} = E_\nu - E_\mu$, U is the anharmonic system–bath interaction [Eq. (1b)] and we sum over the bath final states (β') and average over the initial states (β). Assuming a microcanonical distribution of the bath we have

$$\frac{\Gamma_{b'b',bb}}{\Gamma_{bb,b'b'}} = \frac{S(b')}{S(b)}. \tag{16}$$

Here $S(b')$ and $S(b)$ denote the density of bath states when the system is in the $|b'\rangle$ or $|b\rangle$ state and the bath energy is $E_d - E_{b'}$ or $E_d - E_b$, respectively (E_d being the doorway state energy). When the bath is assumed to have a canonical distribution characterized by a temperature T, Γ satisfies the usual detailed balance condition of the master equation[25]

$$\frac{\Gamma_{b'b',bb}}{\Gamma_{bb,b'b'}} = \exp\left(-\frac{\omega_{b'b}}{kT}\right) \tag{17}$$

with k being the Boltzmann constant. When the system is in the doorway state, the bath is at zero temperature and its density of states is extremely small, i.e., $S(d) \sim 0$. Equation (16) then implies that the vibrational relaxation from the doorway state is irreversible and the reverse rate is negligible. We then postulate the following relaxation matrix:

$$\Gamma_{bb,dd} \equiv \gamma_{bd} \quad (b \neq d), \tag{18a}$$

$$\Gamma_{dd,bb} \equiv \gamma_{db} = 0 \quad (b \neq d), \tag{18b}$$

$$\Gamma_{dd,dd} \equiv -\gamma_d = -\left(\gamma^R + \sum_{b\neq d} \gamma_{bd}\right), \tag{18c}$$

$$\Gamma_{bb,bb} \equiv -\gamma_b = -\left(\gamma^R + \sum_{b\neq d} \gamma_{db}\right) = -\gamma^R \quad (b \neq d). \tag{18d}$$

γ_{bd} is the IVR rate from the doorway state $|d\rangle$ to $|b\rangle$. γ_{db} which represents the reverse rate is taken to be zero. γ_d and γ_b are the total relaxation rate (inverse lifetime) of levels $|d\rangle$ and $|b\rangle$, respectively. γ^R is the inverse radiative lifetime of the electronically excited state. Equations (18) represent a master equation[25] (rate equation) for the vibrational population. For consistency we need to introduce also a relaxation rate for the coherences (off diagonal elements of the density matrix). We, thus, set

$$\Gamma_{\nu\mu,\nu\mu} = \frac{\gamma_\nu + \gamma_\mu}{2}. \tag{18e}$$

The inclusion of Eq. (18e) is essential since relaxation of populations must also affect the coherences, otherwise we obtain an unphysical density matrix. All other matrix elements of Γ not specified in Eqs. (18) are taken to be zero. We reiterate that Eq. (13) holds for any relaxation matrix and it should be straightforward to add relaxation among the $|b\rangle$ levels. We found it unnecessary in the present application to anthracene and we, therefore, consider only the simple relaxation matrix given in Eqs. (18). In the time domain, if we start at $t=0$ in the $|d\rangle$ level, Eqs. (18) will predict the following time evolution:

$$P_d(t) = \exp(-\gamma_d t) \tag{19a}$$

and

$$P_b(t) = \frac{\gamma_{bd}}{\Sigma_{b'\neq d}} \gamma_{b'd} \left[\exp(-\gamma^R t) - \exp(-\gamma_d t)\right], \tag{19b}$$

P_d and P_b being the populations of the doorway state $|d\rangle$ and redistributed state $|b\rangle$ $(b \neq d)$, respectively. Note that

$$\sum_{b\neq d} P_b(t) + P_d(t) = \exp(-\gamma^R t). \tag{20}$$

In Eq. (13) we shall need the inverse of the Γ matrix, which is given by

$$(\Gamma^{-1})_{dd,dd} = -\frac{1}{\gamma_d}, \tag{21a}$$

$$(\Gamma^{-1})_{bb,dd} = -\frac{\gamma_{bd}}{\gamma_d \cdot \gamma^R} \quad (b \neq d), \tag{21b}$$

Eqs. (21) will be used in our simulation of the anthracene spectra in Sec. V.

IV. THE BATH CORRELATION FUNCTIONS—INTRAMOLECULAR DEPHASING

We shall now introduce an explicit model for the bath which will allow us to calculate the dephasing function $J_b^d(t)$ [Eq. (14c)]. Similar model of intramolecular dephasing was introduced in the past for ultracold molecules[6(a)] and for molecular overtones.[26] We shall adopt a harmonic model for the bath and its Hamiltonian is taken to be[18(c)]

$$H_B(Q_B) = |g\rangle h_g \langle g| + |e\rangle h_e \langle e|, \tag{22}$$

where

$$h_g = \frac{1}{2}\sum_{j=1}^{N_B} \Omega_j''(p_j''^2 + q_j''^2 - 1), \tag{23a}$$

$$h_e = \frac{1}{2}\sum_{j=1}^{N_B} \Omega_j'(p_j'^2 + q_j'^2 - 1), \tag{23b}$$

with

$$q_j' = (\Omega_j'/\Omega_j'')^{1/2} q_j'' + \bar{D}_j, \tag{24}$$

and

$$p_j' = [1/(m_j'\Omega_j'\hbar)]^{1/2} P_j', \tag{25a}$$

$$q_j' = [(m_j'\Omega_j'/\hbar)]^{1/2} Q_j'. \tag{25b}$$

We are using here the common spectroscopic notation whereby we denote ground (excited) electronic state quantities with double (single) primes; Q_j, P_j, and m_j are the coordinate, conjugate momentum, and the mass, respectively, of the normal mode j; q_j and p_j are the dimensionless coordinate and momentum, respectively, of the mode j; N_B is the number of bath modes and $\bar{D}_j$ is the dimensionless linear displacement of the jth mode between the ground and the excited electronic states. We are now in a position to evaluate the bath broadening functions. Since initially the molecule is at $T=0$ K, there is no line broadening in absorption. In the dispersed fluorescence experiment considered here (Fig. 1), the bath vibrational energy when the system is in the state $|b\rangle$ is equal to $E_d - E_b$. A statistical treatment of the bath should assume therefore that the bath distribution is microcanonical. The calculation of $J_b^d(t)$ is however greatly simplified when the bath distribution is canonical characterized by a temperature T. In our calculation we have therefore assummed a canonical distribution for the bath. The bath temperature is taken to be the temperature in which the bath energy is equal to $E_d - E_b$. It may be calculated from the equation:

$$E_d - E_b = \sum_{j=1}^{N_B} \bar{n}_j \hbar\Omega_j' = \sum_{j=1}^{N_B} \frac{\hbar\Omega_j'}{\exp(\hbar\Omega_j'/kT) - 1}. \tag{26}$$

It should be noted that at high energies the choice of the bath distribution (canonical or microcanonical) is immaterial. At lower energies Eq. (26) provides a convenient approximation. Once the bath temperature T is determined, we can calculate $J_b^d(t)$. For our model [Eqs. (22)–(25)], $J_b^d(t)$ assumes the form[18(c)]

$$J_b^d(t) = \prod_{j=1}^{N_B} J_j(t), \tag{27}$$

where

$$J_j(t) = [\Psi_j(t)]^{-1/2} \exp[\bar{D}_j^2 \Phi_j(t)] \tag{28}$$

with

$$[\Psi_j(t)] = [1/(4\Omega_j''\Omega_j')](\Omega_j'' C_+ A_- + \Omega_j' C_- A_+) \times (\Omega_j' C_+ A_- + \Omega_j'' C_- A_+), \tag{29}$$

$$\Phi_j(t) = -\Omega_j' C_- A_- / (\Omega_j' C_+ A_- + \Omega_j'' C_- A_+), \tag{30}$$

and

$$C_\pm = 1 \pm \exp(-i\Omega_j'' t), \tag{31a}$$

$$A_\pm = (\bar{n}_j + 1) \pm \bar{n}_j \exp(i\Omega_j' t), \tag{31b}$$

$$\bar{n}_j = [\exp(\hbar\Omega_j'/kT) - 1]^{-1}, \tag{31c}$$

where $\bar{n}_j$ is the mean occupation number of the jth bath mode when the system is in the electronically excited state at temperature T. Equations (28)–(31) may be obtained from Eqs. (120)–(121) of Ref. 18(c) by interchanging Ω' and Ω''. We have further made the following simplifying assumptions regarding the bath. First, since the bath is weakly coupled to the electronic transition, we set $\bar{D}_j = 0$ (no linear displacements). The ground state bath frequencies Ω_j'' are known (see Table II). The excited state frequencies Ω_j' were evaluated using the following procedure. We introduced the variables

$$\alpha_j = (\Omega_j'' - \Omega_j')/\Omega'', \tag{32}$$

α_j represents the relative frequency change of the jth bath mode upon electronic excitation. Ω_j' is usually smaller than Ω_j'', which implies weaker bonds in the electronically excited state. In the present model α_j will be responsible for the line broadening (dephasing) and the red shift observed in the fluorescence spectra relative to the absorption. Since α_j is not available we shall adopt a statistical approach[18(c),27] and replace α_j's by a random variable α with a Gaussian distribution

$$P(\alpha)=\begin{cases}\sqrt{\frac{2}{\pi}}\frac{1}{\sigma}\exp\left(-\frac{\alpha^2}{2\sigma^2}\right) & (\alpha\geqslant 0)\\ 0 & (\alpha<0)\end{cases} \tag{33}$$

with the normalization

$$\int_0^\infty P(\alpha)d\alpha=1. \tag{33a}$$

σ is the variance of the distribution and $\langle\alpha\rangle$ is the mean relative frequency change upon electronic excitation

$$\langle\alpha\rangle=\sqrt{\frac{2}{\pi}}\sigma\approx 0.08\sigma. \tag{33b}$$

In our calculations α_j were generated by a Gaussian random generator routine. Since Ω_j'' are known, we then have $\Omega_j'=\Omega_j''(1-\alpha_j)$. Ω_j' obtained this way together with Ω_j'', and the temperature T [Eq. (26)] were substituted in Eqs. (27)–(31) to get $J_b^d(t)$. In the calculations presented in Sec. V we repeated the random sampling for α_j ten times and $J_b^d(t)$ was taken to be the ensemble average of these ten calculations.

TABLE I. In plane vibrational frequencies of the ground electronic state (S_0) of anthracene (Refs. 9 and 28).

Mode	ω'' (cm^{-1})	Mode	ω'' (cm^{-1})
a_g		b_{1u}	
1	3088	1	3100
2	3057	2	3049
3	3053	3	3022
4	1566[a]	4	1620
5	1486[a]	5	1448
6	1408[a]	6	1316
7	1263[a]	7	1274
8	1165[a]	8	1150
9	1012[a]	9	907
10	753[a]	10	651
11	624[a]	11	244
12	390[a]		
b_{3g}		b_{2u}	
1	3063	1	3079
2	3006	2	3048
3	1643[a]	3	1533
4	1576[a]	4	1462
5	1382[a]	5	1398
6	1274	6	1346
7	1183[a]	7	1169
8	1100[a]	8	1125
9	912[a]	9	999
10	524[a]	10	812
11	391[a]	11	615

[a] System modes.

TABLE II. Out of plane vibrational frequencies of the ground electronic state (S_0) of anthracene (Ref. 29).

Mode	ω'' (cm^{-1})	Mode	ω'' (cm^{-1})
b_{3u}		b_{1g}	
1	819	1	774
2	729	2	578
3	556	3	403
4	416	4	220
5	337		
6	90		
a_u		b_{2g}	
1	859	1	910
2	787	2	801
3	656	3	682
4	481	4	602
5	124	5	510
		6	287

V. APPLICATION TO ANTHRACENE

Zewail and co-workers have carried out detailed studies of jet cooled anthracene using detection which is both time resolved (on a picosecond time scale) and frequency resolved.[9,10] These studies make this molecule most suitable for our theoretical analysis. The dispersed fluorescence spectra of anthracene can be divided into three groups depending on the magnitude of the excess vibrational energy. In anthracene we have low energy spectra ranging from 0 to 1200 cm^{-1}, intermediate energy spectra from 1200 to 1600 cm^{-1}, and high energy spectra for excess energies great than 1600 cm^{-1}. This classification is based on the degree of spectral congestion as well as the time evolution of the fluorescence spectra. In the low energy region there is no IVR and the fluorescence decays with the radiative lifetime. In the intermediate region the time evolution shows quantum beats which are a signature of few coupled vibronic levels and a reversible vibrational redistribution. Finally, the high energy region is characterized by the onset of irreversible IVR with a 22 ps time scale. Anthracene ($C_{14}H_{10}$) has 66 normal modes. The ground state frequencies of all the modes are available from spectroscopic studies and theoretical calculations,[9,28,29] and are listed in Tables I and II. Previous spectroscopic studies[28,29] in the gas phase, matrices, pure crystal, and the supersonic beam data[9] show 17 modes (nine totally symmetric a_{1g} modes and eight b_{3g} modes) which are strongly coupled to the electronic transition and are optically active. Consequently we have chosen these to be the system modes. For the system modes we have adopted a harmonic model, i.e.,

$$H_g=\frac{1}{2}\sum_{j=1}^{N_S}\omega_j''(p_j''^2+q_j''^2-1), \tag{34a}$$

$$H_e=\frac{1}{2}\sum_{j=1}^{N_S}\omega_j'(p_j'^2+q_j'^2-1), \tag{34b}$$

with

$$q_j'=\sqrt{\omega_j'/\omega_j''}q_j''+D_j, \tag{34c}$$

where the notation is the same as Eq. (23) with ω_j being the frequency of the jth system mode, and N_S being the number

TABLE III. Vibrational frequencies and dimensionless displacements of the system modes of anthracene (Ref. 9).

Mode	ω'' (cm^{-1})	ω' (cm^{-1})	D
a_g			
4	1566	1501	0.80
5	1486	1420	0.20
6	1408	1380	1.35
7	1263	1168	0.69
8	1165	1163	0.67
9	1012	1019	0.20
10	753	755	0.24
11	624	583	0.21
12	390	385	0.79
b_{3g}			
$\bar{3}$	1643	1635	0.63
$\bar{4}$	1576	1514	0.35
$\bar{5}$	1382	1409	0.20
$\bar{7}$	1184	1183	0.24
$\bar{8}$	1100	1046	0.15
$\bar{9}$	912	889	0.20
$\bar{10}$	524	473	0.15
$\bar{11}$	391	232	0.71

of the system modes. The system modes are marked by a in Table I. The spectroscopic information on the system modes (ω_j'', ω_j', and D_j) is available[9,28,29] and is given in Table III. The values of D_j were adjusted to reproduce the experimental emission spectra from the 0^0 level. We have calculated the total density of vibrational states and the bath density of states by a direct counting, and the results are shown in Fig. 3.

In order to calculate the dispersed fluorescence using Eq. (13), we need to evaluate the system line shape function $T_{bb}(t)$, the bath dephasing function $J_b^d(t)$, and the IVR matrix Γ. We have first calculated the dispersed fluorescence assuming no IVR and setting $\Gamma_{bb,dd} = \gamma^R \delta_{b,d}$. In this case all the emission originates from the doorway state. The bath modes do not play any role in this limit since the bath remains cold during the entire fluorescence process. The only quantity needed in the calculation is $T_{dd}(t)$. A comparison of these calculations with the experimental data allows us to illustrate the effects of IVR. In our calculations we further invoke the Condon approximation and assume that the electronic dipole operator is independent on the molecular coordinates, i.e., $\mu(Q_S) = \mu$. We have derived previously an explicit expression for $T_{bb}(t)$ for the model Hamiltonian [Eq. (34)].[18(b)] That expression is eigenstate free in the sense that it has the form of a product of contributions from

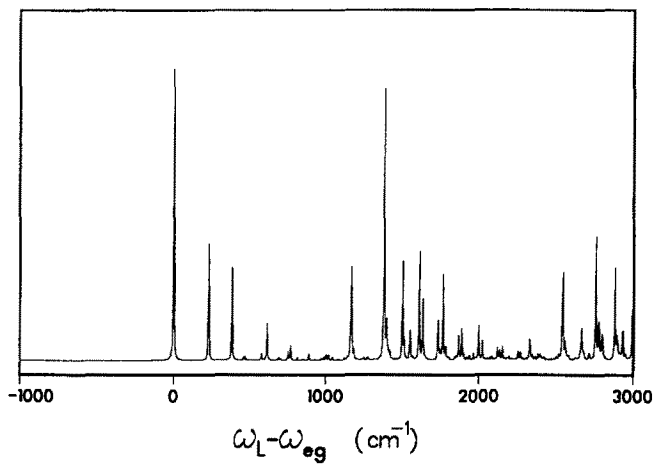

FIG. 4. The calculated absorption spectrum of jet-cooled anthracene, using the 17 system modes (Table III). The calculation was made using Eqs. (22a), (32), and (33) of Ref. 18(b).

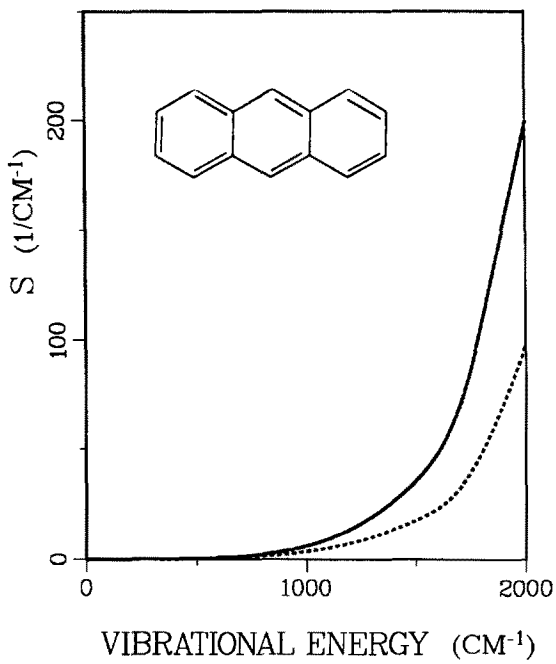

FIG. 3. The total density of vibrational states of anthracene (solid line) and the bath (49 modes) density of states (dashed line) for the electronically excited S_1 state of anthracene. The excited state bath frequencies were calculated using the procedure outlined in Sec. IV by using the available ground state frequencies and using the distribution $P(\alpha)$ of frequency differences [Eq. (33)] with $\sigma = 0.08$.

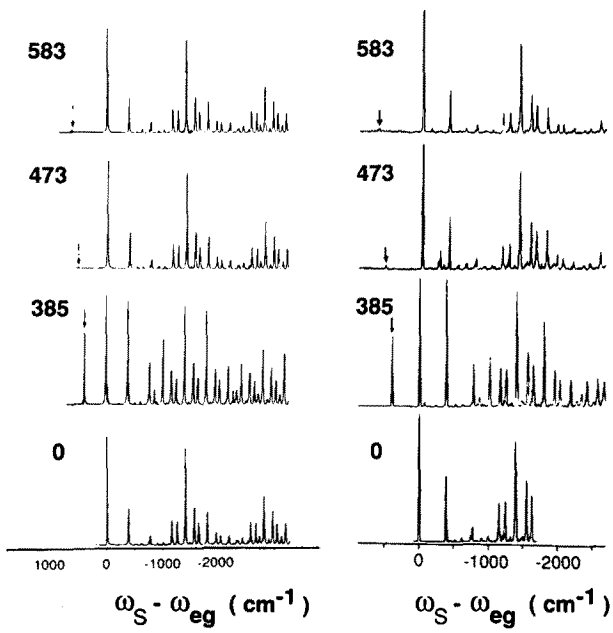

FIG. 5. Comparison of our harmonic model calculations of the fluorescence spectra of jet-cooled anthracene in the low energy region (left panel) with experiment (Ref. 9) (right panel). The arrow in each spectrum indicates the laser excitation position. ω_j'', ω_j', and D_j used in the calculations for the 17 system modes are listed in Table III. The bath modes do not enter in these calculations. Calculations were made using Eq. 11(d) of Ref. 18(b).

single modes and its evaluation does not involve any summation over molecular eigenstates. $T_{bb}(\tau)$ was calculated at $M = 8192$ points with a time interval $\Delta t = 2\pi/(M\Delta\omega)$, where $\Delta\omega = 2\ \mathrm{cm}^{-1}$ is the spectral resolution of our calculation. A standard fast Fourier transform routine was then used to perform the integration [Eq. (14a)] and obtain $T_{bb}(\omega)$. Figure 4 shows the absorption spectrum of ultracold anthracene calculated using the ground and excited state frequencies and dimensionless displacements of the 17 system modes (Table III). The absorption spectrum was calculated using the following expression[18(b)]:

$$\sigma(\omega_L) = -2\ \mathrm{Im}\ T'_{00}(\omega_L), \tag{35}$$

where $T'(\omega)$ is similar to $T(\omega)$ [Eqs. (14)] except that H_g is replaced by H_e and $J_b^d(\tau)$ is set to unity (the bath is cold). The state $|0\rangle$ is the ground vibronic state of $|g\rangle$. In Figs. 5 and 6 we compare our calculations of the fluorescence spectra with experiments in the low energy region. The excellent agreement for the five lowest energy levels (from 0 up to 766 cm^{-1}) indicates the absence of energy flow out of the initially excited doorway state, i.e., the absence of IVR, and the emission comes exclusively from the doorway state. This can be easily rationalized by the low density of states of the bath in this region. The three calculated higher energy spectra (889, 1019, and 1168 cm^{-1}) also show good agreement with experiment in terms of the peak positions and relative intensities. But the experimental spectra show the onset of line broadening, which is clearly absent in our harmonic calculations.

Turning to the intermediate energy region (Fig. 7), we notice considerable differences between the harmonic model calculations and the experimental spectra, where the Raman (unredistributed) component decreases dramatically, and the relaxed fluorescence is very significant. The coexistence of Raman and relaxed fluorescence implies that the doorway state is coupled with a limited number of vibrational levels within that energy region. This is confirmed by the time resolved experiments in this energy range. Consider for example, the 6^1 (1380 cm^{-1}) level. The harmonic spectrum consists of the 6_n^1 progression as well as $A\,{}_m^m$ progressions where A is any of the system modes. The mixing of the 6^1 level via anharmonicities will populate bath modes and the emission spectrum will contain also sequences of the type $B\,{}_n^n$ where B is some bath mode and the bath optical transitions are assumed to be diagonal. Since the bath excited state frequencies Ω_j' are different from the ground state frequencies Ω_j'', the $B\,{}_n^n$ transitions will have a slightly different transition frequency which will vary with B and with n. These sequences will result in the broad emission which is observed experimentally.[6(a)] In the high energy region (Fig. 8) the redistributed emission becomes dominant and the sharp Raman lines disappear. The high density of vibrational states in this region results in the establishment of fast irreversible IVR processes (time scale ~ 22 ps) as is clearly seen in the time resolved spectra.[10] Figures 5–8 demonstrate how the effect of IVR and dephasing introduced by the bath increase

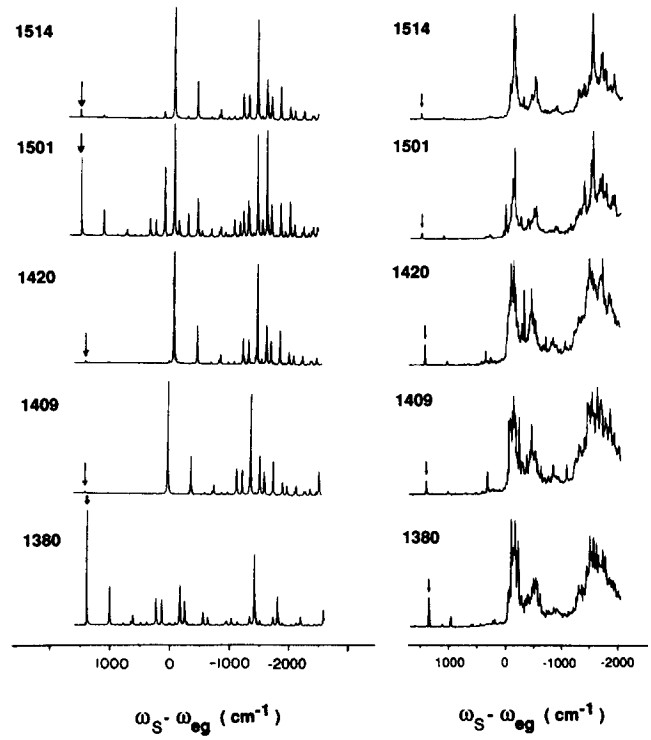

FIG. 7. Same as Fig. 5. for the intermediate energy region.

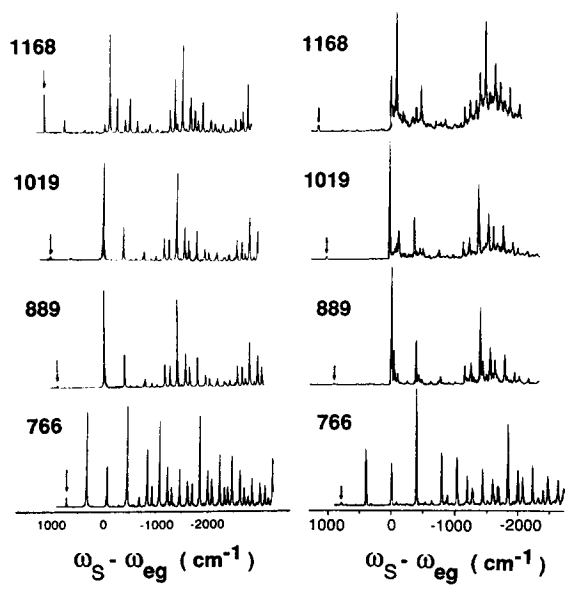

FIG. 6. Same as Fig. 5 for higher excitation energies of the low energy region.

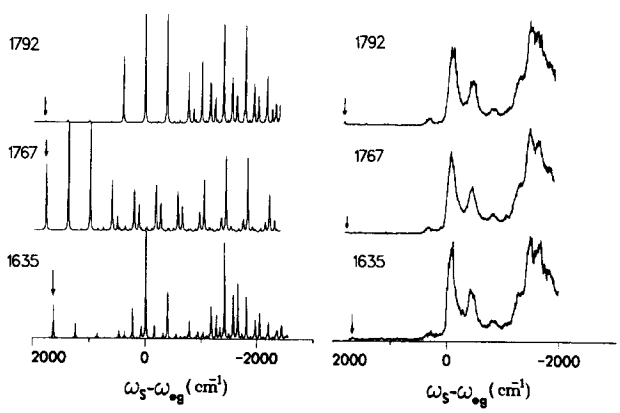

FIG. 8. Same as Fig. 5 for the high energy region.

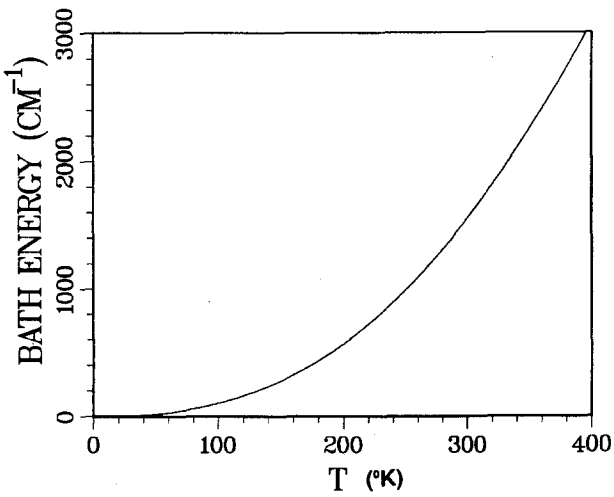

FIG. 9. The mean bath energy versus the bath temperature T calculated using Eq. (26). The bath frequencies in S_1 were calculated using the S_0 frequencies of Tables I and II and Eq. (33) with $\sigma = 0.08$.

dramatically with the excess vibrational energy.

We shall now introduce the bath and incorporate the dephasing $J_b^d(t)$ and the IVR matrix Γ in the calculations. In our subsequent calculations we shall focus on the high energy region (region III) in which the usage of the master equation of Sec. III to describe the IVR is fully justified. For each level $|b\rangle$ the bath temperature was calculated using Eqs. (26) and $J_b^d(t)$ was then evaluated using Eqs. (27)–(34). The bath temperature T vs the excess vibrational energy E [Eq. (26)] is shown in Fig. 9. The IVR matrix Γ was defined in Eq. (18). In order to simplify the calculation we have divided the 49 bath modes into 10 groups with the following frequencies: 80, 110, 200, 400, 600, 800, 1000, 1200, 1400, and 3000 cm^{-1} and the number of modes in each group was 1, 1, 2, 7, 7, 8, 5, 5, 4, and 9, respectively. This grouping is consistent with our statistical treatment of the bath in which we keep only global features and not the fine details of the bath. We shall define the bath spectral density

$$J(\omega) = \int_{-\infty}^{+\infty} d\tau\, J_b^d(\tau)\exp(i\omega\tau). \tag{36}$$

The frequency change parameter σ determines both the line broadening and the red shift of the emission spectra. In Fig. 10 we display the bath spectral density [Eq. (36)] for three bath temperatures (100, 316, and 600 K) and for three values of σ(0.03,0.08,0.12). Note the different frequency and intensity scales of the various panels in Fig. 10. In Fig. 11 we show the emission from the level 0^0 with a bath temperature of 316 K for various values of σ as indicated. Figures 10 and 11 demonstrate how the emission is broadened and red shift-

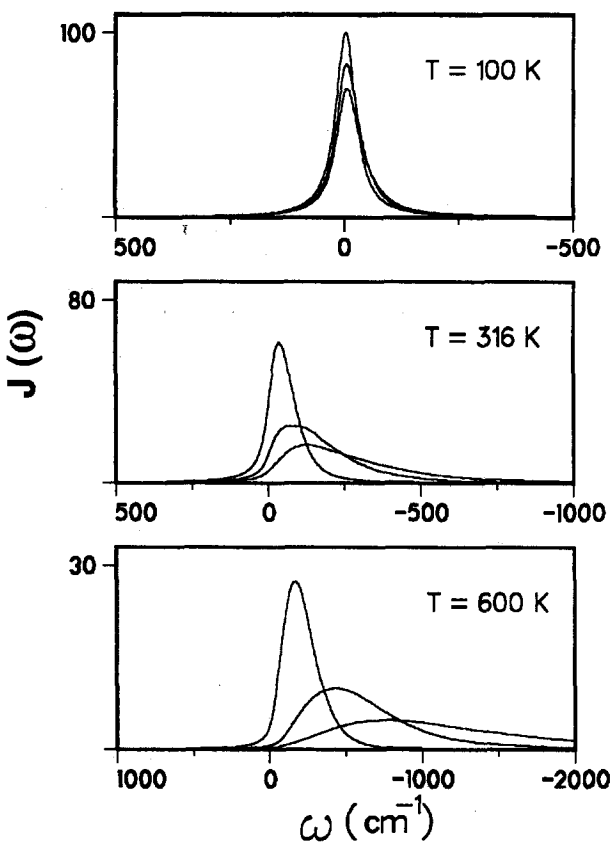

FIG. 10. The bath spectral density [Eq. (36)] for the fluorescence emission at three temperatures: 100, 316, and 600 K. Each panel consists of three curves with different values of σ: 0.03, 0.08, and 0.12 for the narrow, intermediate, and the broad curves, respectively. Note the change in frequency and intensity scale in the various panels. As the temperature and σ increase the spectral density broadens, and is red shifted.

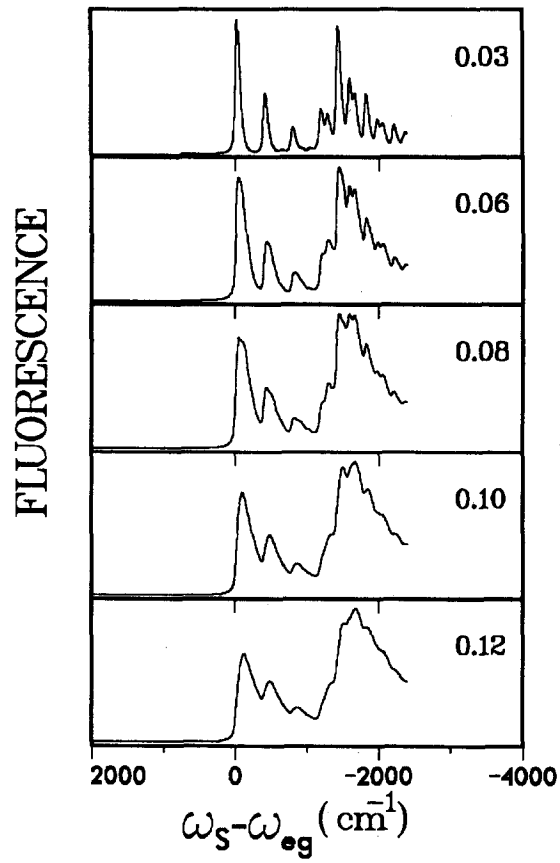

FIG. 11. The calculated 0^0 fluorescence emission spectra of anthracene for bath temperature $T = 316$ K (corresponding to bath vibrational energy of 1792 cm^{-1}) and $\sigma = 0.03, 0.06, 0.08, 0.10, 0.12$ as indicated. Note the increased broadening and red shift as σ increases.

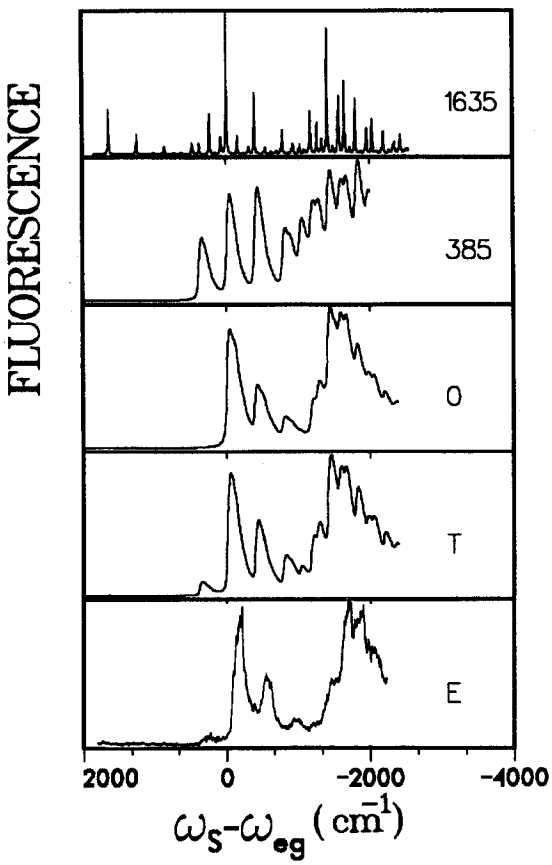

FIG. 12. The calculated dispersed fluorescence spectrum of ultracold anthracene following excitation of the $\bar{3}^1$ (1635 cm^{-1}) level. We assumed that two system vibronic levels in S_1 are accessible via IVR from the doorway state: 12^1 (385 cm^{-1}) and 0^0 (0 cm^{-1}). The top panel shows the direct emission from the doorway state in which the bath is cold and does not play any role. The following two panels show the emission from the 12^1 and 0^0 levels with bath temperature 172 and 306 K, respectively. The total emission [Eq. (13)] is given by a superposition of these three spectra with a relative weight determined by the IVR matrix. The bottom two panels show our best theoretical fit (labeled T) and the experiment[9] labeled E. Our best fit (Table IV) corresponds to an IVR time scale of 200 and 11 ps for relaxation to the 12^1 and the 0^0 level, respectively.

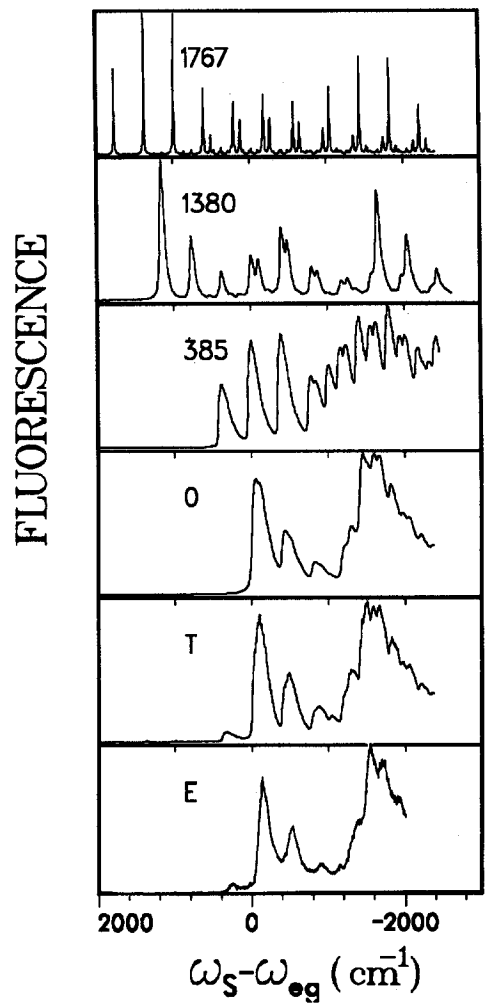

FIG. 13. The calculated dispersed fluorescence spectrum of ultracold anthracene following excitation of the $12^1\,6^1$ (1767 cm^{-1}) level. We assumed that three system vibronic levels in S_1 are accessible via IVR from the doorway state: 6^1 (1380 cm^{-1}), 12^1 (385 cm^{-1}), and 0^0 (0 cm^{-1}). The top panel shows the direct emission from the doorway state in which the bath is cold and does not play any role. The following three panels show the emission from the 6^1, 12^1, and 0^0 levels with bath temperature 172, 286, and 316 K, respectively. The total emission [Eq. (13)] is given by a superposition of these spectra with a relative weight determined by the IVR matrix. We found that inclusion of the level 6^1 did not improve the fit and did not include it in our final fit. The bottom two panels show our best theoretical fit (labeled T) and the experiment (Ref. 9) labeled E. Our best fit (Table IV) corresponds to an IVR time scale of 200 and 11 ps for relaxation to the 12^1 and the 0^0 levels, respectively.

ed as σ increases. In the fits to the experiment shown in Figs. 12–14 we found the value of $\sigma = 0.08$ to provide the best agreement with the observed width and red shift (with respect to the absorption). This value corresponds to $\langle\alpha\rangle = 0.064$ [Eq. (33b)], which implies that the frequencies in the excited state are on the average 6.4% lower than those in the ground state. In Fig. 12 we display our calculations for the emission from the $\bar{3}^1$ (1635 cm^{-1}) level. In our calculations we assumed that this state relaxes to the 0 (vibrationless) state of the system. In addition we also assumed relaxation to the 12^1 (385 cm^{-1}) state. This will account for the weak feature at 385 cm^{-1} to the blue of the 0–0 emission. Note also that the 12 mode has a large displacement $D_{12} = 0.79$. We, thus, assumed an IVR relaxation matrix with three states: the doorway state and the two states introduced above. The top panel in Fig. 12 shows the emission from the doorway state. The bath is cold and does not play any role in the spectrum. The next panel shows emission from the 12^1 state (385 cm^{-1}) with bath temperature of 275 K and $\sigma = 0.08$, and the third panel shows emission from the 0^0 state with bath temperature of 307 K and $\sigma = 0.08$. Our theoretical calculation [(Eq. 13)] is a superposition of these three spectra with a relative weight determined by the IVR matrix Γ. The optimal values of the IVR rates (γ_{bd}/γ^R) are listed in Table IV, and the best fit is shown in the next panel labeled T. The lowest panel shows the experimental dispersed fluorescence.[9] Our calculation results in γ_{bd}/γ^R. If we assume that the decay in the low energy region is purely radiative we have[10(a)] $\hbar/\gamma^R = 20$ ns. Our calculations thus represent an IVR time scale of 200 and 11 ps for relaxation to the 12^1 and the 0^0 levels, respectively. In Fig. 13 we perform similar calculations for emission from the $12^1 6^1$ (1767 cm^{-1}) level. In this case we considered IVR to the 6^1 (1380 cm^{-1}) level in addition to the two levels used in Fig. 12.

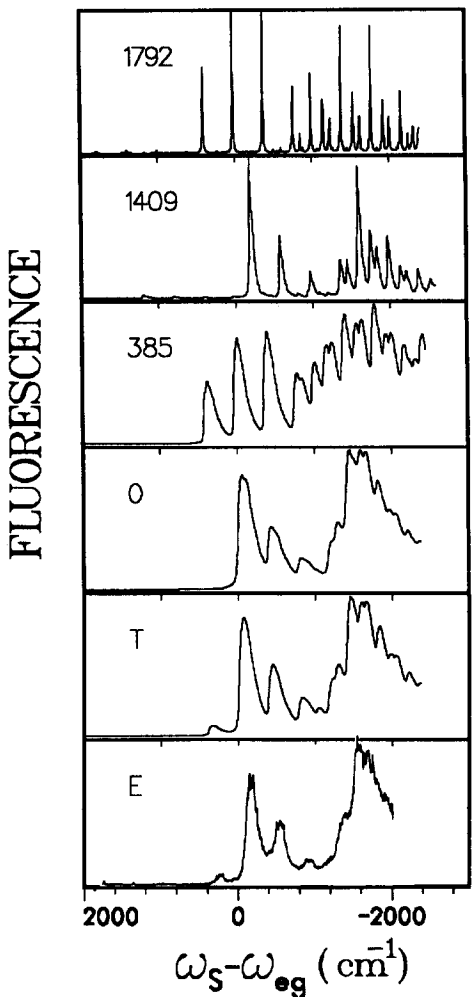

FIG. 14. The calculated dispersed fluorescence spectrum of ultracold anthracene following excitation of the $12^1\,\bar{5}^1$ (1792 cm^{-1}) level. We assumed that three system vibronic levels in S_1 are accessible via IVR from the doorway states: $\bar{5}^1$ (1380), 12^1 (385), and 0^0 (0 cm^{-1}). The top panel shows the direct emission from the doorway state in which the bath is cold and does not play any role. The following three panels show the emission from the $\bar{5}^1$, 12^1, and 0^0 with bath temperature 172, 286, and 318 K, respectively. The total emission [Eq. (13)] is given by a superposition of these spectra with a relative weight determined by the IVR matrix. We found that inclusion of the $\bar{5}^1$ level did not improve the fit and then did not include it in our final fit. The bottom two panels show our best theoretical fit (labeled *T*) and the experiment (Ref. 9) labeled *E*. Our best fit (Table IV) corresponds to an IVR time scale of 133 and 11 ps for relaxation to the 12^1 and the 0^0 levels, respectively.

12. However the inclusion of the 6^1 level did not improve our final fit. The top four panels show the emission from the 1767, 1380, 385, and 0 cm^{-1} levels with bath temperature of 0, 172, 286, and 316 K, respectively, and $\sigma = 0.08$. The best values of γ_{bd}/γ^R are listed in Table IV and assuming radiative lifetime $\hbar/\gamma^R = 2\times 10^4$ ps, we get IVR time scale of 200 and 11 ps to the 12^1 and 0^0 levels respectively. In Fig. 14 we repeat this procedure for the $12^1\bar{5}^1$ (1792 cm^{-1}) level. We assumed IVR to levels $\bar{5}^1$, 12^1, and 0^0 with bath temperatures of 172, 288, and 318 K, respectively. Again the inclusion of the $\bar{5}^1$ level did not improve our final fit. We found the IVR time scales to be 133 and 11 ps for relaxation to the 12^1 and the 0^0 levels, respectively. In Fig. 15 we display the best fits obtained in Figs. 12–14 (dashed curve) superimposed on the experimental spectra (solid curve). The agreement is very good and we are able to reproduce these spectra quantitatively.

TABLE IV. Relative IVR rates γ_{db}/γ^R for the high energy region in anthracene.

$\|b\rangle$	$\|d\rangle = 12^1\bar{5}^1$ (1792 cm^{-1})	$\|d\rangle = 12^16^1$ (1767 cm^{-1})	$\|d\rangle = \bar{3}^1$ (1635 cm^{-1})
12^1 (385 cm^{-1})	150	100	100
0^0 (0 cm^{-1})	1750	1800	1800

VI. CONCLUDING REMARKS

In this article we developed a *reduced description* suitable for the calculation of dispersed fluorescence line shapes of ultracold anharmonic molecules. Our simulations of the spectra of anthracene provide a quantitative interpretation for the observed line shapes[9,10] and allow us to extract IVR rates from the frequency resolved spectra. In addition we can interpret the intramolecular dephasing processes which dominate the observed line shapes and predict their variation with the excess vibrational energy. The main characteristics of these spectra is the coexistence of progressions of narrow lines (direct emission) and broad (redistributed) emission. The relative magnitude of these two components is determined by the IVR processes. In the absence of IVR processes, we see only the direct emission (see Figs. 5 and 6). The IVR populates the bath states and their thermal fluctuations result in the broad emission (dephasing processes). The infrared emission spectra of McDonald and co-workers yield complimentary information regarding IVR in the

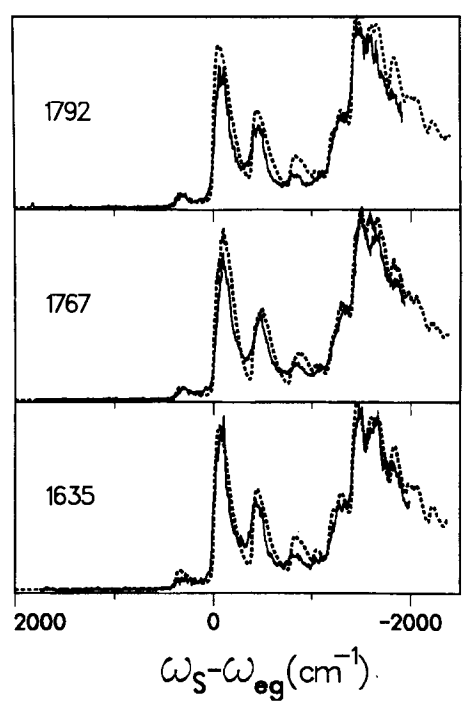

FIG. 15. Direct comparison of our theoretical calculations (curves *T* in Figs. 12–14) and experimental results for fluorescence of anthracene in the high energy region. Solid lines, experimental (Ref. 9). Dashed lines, calculations. The excess vibrational energy of the doorway state is indicated in each panel.

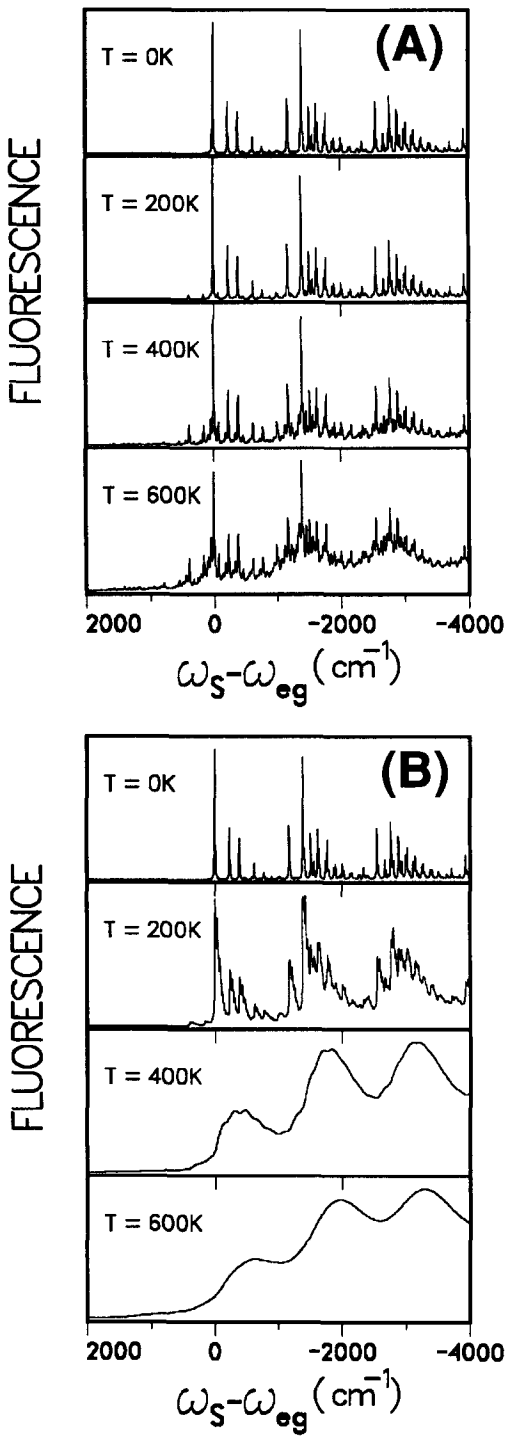

FIG. 16. The calculated emission spectra of anthracene when the molecular vibrations are equilibrated with an heat bath at different temperatures from 0 up to 600 K, as indicated. (A) Using only the 17 system modes (Table III). (B) Using all the 66 modes. The bath was included using our statistical model with $\sigma = 0.08$.

ground electronic state.[30] The coexistence of narrow and broad emission is a common phenomenon in the fluorescence studies of crystals at finite temperatures (gas phase, solutions, and crystals).[14,19,21] In that case vibrational relaxation processes are not needed in order to induce the broad emission. Thermal fluctuations of the bath (whether intramolecular or intermolecular) exist in the absence of IVR and induces dephasing. Denoting the dephasing rate [i.e., the width of the bath spectra density, Eq. (36)] by $\hat{\Gamma}$ and the excited state lifetime by γ, the ratio of the redistributed to the direct emission is $\hat{\Gamma}/\gamma$.[18(c),19] As the lifetime shortens, γ increases, and the narow emission becomes dominant. The narrow component is called Raman and the broad component is called fluorescence. In Fig. 16 we show the emission of anthracene at several temperatures in the absence of IVR. This was calculated using our eigenstate-free expression [Eqs. (22a), (32), and (33) in Ref. 18(b)]. In Fig. 16(A) we included only the 17 system modes in the calculating whereas in Fig. 16(B) we included the bath modes as well using the procedure outlined in Sec. IV with $\sigma = 0.08$. As the temperature increases the dephasing rate $\hat{\Gamma}$ increases. This results in increasing $\hat{\Gamma}/\gamma$ (since the excited state radiative width γ is fixed). Consequently, the Raman component gradually disappears with temperature and the fluorescence component becomes dominant.

In conclusion, we note that the present theory applies also to the chemical timing spectroscopy of Parmenter *et al.*[12] which is based on adding a quencher which shortens the excited state lifetime and increases γ. The experiments show the enhancement of the narrow emission (compared with the broad background) with the quencher concentrations for *p*-difluorobenzene and *p*-fluorotoluene. These results are usually interpreted to show an evidence for IVR processes which occur on picosecond time scales. The present theory shows that another mechanism for the narrowing of the short time emission is the competition between Raman and fluorescence spectra where intramolecular dephasing (rather than vibrational relaxation) is the cause of the broadening, since increasing γ for a fixed dephasing rate $\hat{\Gamma}$ will decrease the fluorescence and enhance the Raman component. A more detailed analysis of these experiments is needed in order to determine the relative contribution of dephasing and IVR processes in these spectra. This ambiguity does not exist for ultracold molecules in which the broad emission is clearly induced by IVR.

ACKNOWLEDGMENTS

The support of the National Science Foundation, the Office of Naval Research, the US Army Research Office, and the Petroleum Research Fund, administered by the American Chemical Society, is gratefully acknowledged. We wish to thank Professor A. H. Zewail for useful discussions.

APPENDIX: DERIVATION OF EQ. (13)

Starting with Eqs. (10) we shall write explicitly the averaging over the bath.

$$\mathcal{T}_I = |\mu_{ad}\,\mu_{dc}|^2 \exp[i\omega_S t_3 - i(\omega_L - \omega_S)t_2 - i\omega_L t_1] \times \sum_{\alpha,\alpha',\alpha_1,\alpha_2,\alpha_3,\alpha_4} \langle\langle {}^{\alpha\alpha'}_{dc}|\mathcal{G}(t_3)|{}^{\alpha_3\alpha_4}_{dc}\rangle\rangle \times \langle\langle {}^{\alpha_3\alpha_4}_{ac}|\mathcal{G}(t_2)|{}^{\alpha_1\alpha_2}_{ac}\rangle\rangle \langle\langle {}^{\alpha_1\alpha_2}_{ad}|\mathcal{G}(t_1)|{}^{\alpha\alpha}_{ad}\rangle\rangle \rho_g(\alpha), \quad \text{(A1a)}$$

$$\mathscr{T}_{\rm II} = \sum_b |\mu_{ad}\mu_{bc}|^2 \exp(i\omega_S t_3 - i\omega_L t_1) \times \sum_{\alpha,\alpha',\alpha_1,\alpha_2,\alpha_3,\alpha_4} \langle\langle {}^{\alpha\alpha'}_{bc}|\mathscr{G}(t_3)|{}^{\alpha_3\alpha_4}_{bc}\rangle\rangle \times \langle\langle {}^{\alpha_3\alpha_4}_{bb}|\mathscr{G}(t_2)|{}^{\alpha_1\alpha_2}_{dd}\rangle\rangle\langle\langle {}^{\alpha_1\alpha_2}_{ad}|\mathscr{G}(t_1)|{}^{\alpha\alpha}_{ad}\rangle\rangle\rho_g(\alpha), \quad \text{(A1b)}$$

$$\mathscr{T}_{\rm III} = \sum_b |\mu_{ad}\mu_{bc}|^2 \exp(-i\omega_S t_3 - i\omega_L t_1) \times \sum_{\alpha,\alpha',\alpha_1,\alpha_2,\alpha_3,\alpha_4} \langle\langle {}^{\alpha\alpha'}_{bc}|\mathscr{G}(t_3)|{}^{\alpha_3\alpha_4}_{cb}\rangle\rangle \times \langle\langle {}^{\alpha_3\alpha_4}_{bb}|\mathscr{G}(t_2)|{}^{\alpha_1\alpha_2}_{dd}\rangle\rangle\langle\langle {}^{\alpha_1\alpha_2}_{ad}|\mathscr{G}(t_1)|{}^{\alpha\alpha}_{ad}\rangle\rangle\rho_g(\alpha), \quad \text{(A1c)}$$

Here $|a\alpha_1\rangle$ denotes a direct product of a system state $|a\rangle$ and the bath state $|\alpha_1\rangle$ and $|{}^{\alpha_1\alpha_2}_{ac}\rangle\rangle$ is the Liouville space vector corresponding to $|a\alpha_1\rangle\langle c\alpha_2|$. The diagonal matrix elements of $\mathscr{G}(\tau)$ are

$$\begin{aligned}\mathscr{G}_{\nu\lambda,\nu\lambda}(\tau) &= \langle\langle \nu\lambda|\mathscr{G}(\tau)|\nu\lambda\rangle\rangle_S \\ &= \langle\langle \nu\lambda|\exp[-i\mathscr{L}\tau]|\nu\lambda\rangle\rangle_S \\ &\equiv I_{\nu\lambda}(\tau). \end{aligned} \quad \text{(A2)}$$

Hereafter we denote the total inverse lifetime of state $|\nu\rangle$ by γ_ν [see Eq. (18)]. We further define

$$\Gamma_{\nu\lambda} = 1/2(\gamma_\nu + \gamma_\lambda) \quad \text{(A3)}$$

and

$$I_{\nu\lambda}(\tau) \equiv \exp[-i\omega_{\nu\lambda}\tau - \Gamma_{\nu\lambda}|\tau|] \quad (\nu \neq \lambda), \quad \text{(A4)}$$

$$\omega_{\nu\lambda} \equiv E_\nu - E_\lambda, \quad \text{(A4a)}$$

$$\mathscr{G}_{dd,dd}(\tau) = \langle\langle dd|\exp(-\Gamma\tau)|dd\rangle\rangle, \quad \text{(A5a)}$$

$$\mathscr{G}_{bb,dd}(\tau) = \langle\langle bb|\exp(-\Gamma\tau)|dd\rangle\rangle \quad (b \neq d). \quad \text{(A5b)}$$

We shall now introduce the factorization approximation which will enable us to evaluate $\mathscr{T}_{\rm I}$, $\mathscr{T}_{\rm II}$, and $\mathscr{T}_{\rm III}$. We first introduce the Liouville space projection operator[19,21]

$$\hat{P} = |gg\rangle\rangle\langle\langle gg|\rho_g\,{\rm Tr}_B + \sum_b |bb\rangle\rangle\langle\langle bb|\rho_b\,{\rm Tr}_B, \quad \text{(A6)}$$

where ρ_g is the zero temperature density matrix of the bath in the ground electronic state; and ρ_b is the bath density matrix when the system is in the state $|b\rangle$. The summation runs over all of the vibrational states with the energy E_b less than E_d in the excited electronic state $|e\rangle$. By replacing $\mathscr{G}(t_2)$ in Eqs. (8) by $\hat{P}\mathscr{G}(t_2)\hat{P}$ the average of product of Green's functions can be replaced by the product of averaged Green's functions, and we get[18,21]

$$\begin{aligned} S_d(\omega_S) = 2\,{\rm Re}\sum_{b,c}\int_0^\infty dt_1\int_0^\infty dt_2\int_0^\infty dt_3 \times\{&[|\mu_{ad}\mu_{dc}|^2 I_{dc}(t_3)I_{ac}(t_2)I_{ad}(t_1)J_g(t_3)J_g^*(t_1)\exp[i\omega_S t_3 - i(\omega_L-\omega_S)t_2 - i\omega_L t_1] \\ &+ |\mu_{ad}\mu_{bc}|^2 I_{bc}(t_3)\mathscr{G}_{bb,bb}(t_2)I_{ad}(t_1)J_b^*(t_3)J_g^*(t_1)\exp[i\omega_S t_3 - i\omega_L t_1] \\ &+ I_{bc}(t_3)\mathscr{G}_{bb,dd}(t_2)I_{ad}(t_1)J_b(t_3)J_g^*(t_1)\exp(-\omega_S t_3 - i\omega_L t_1)]\}. \end{aligned} \quad \text{(A7)}$$

Here $S_d(\omega_S)$ denotes the emission from a particular doorway state $|d\rangle$. We have defined the bath line broadening functions for absorption when the system is initially in the ground electronic state $|g\rangle$:

$$J_g(t) = {\rm Tr}_B[\exp(ih_g t)\exp(-ih_e t)\rho_g] \quad \text{(A8a)}$$

and the bath emission line broadening function when the system is initially in the $|b\rangle$ state:

$$J_b^d(t) = {\rm Tr}_B[\exp(ih_e t)\exp(-ih_g t)\rho_b]. \quad \text{(A8b)}$$

Here ${\rm Tr}_B$ represents the trace over the bath degrees of freedom. Since the bath is initially cold we may assume $J_g(t) \approx 1$. When the bath is infinite (e.g., solvent) it is possible to use the following projection operator[13,14,23] instead of Eq. (A6):

$$P = \rho_{\rm Bath}\,{\rm Tr}_B. \quad \text{(A9)}$$

In this case the bath is weakly correlated and is unaffected by the system and the factorization approximation yields an expression similar to Eq. (A7) but where all broadening functions $J_g(t)$ and $J_b^d(t)$ are equal, independent of b or d. The projection operator (A6) keeps track of the correlated dynamics of the system and the bath. Each vibronic state of the system has a different bath distribution (ρ_g or ρ_b) associated with it. This is crucial for an adequate description of supersonic beam line shapes. The dispersed fluorescence can be recast in the following form:

$$\begin{aligned} S_d(\omega_S) &= -2\,{\rm Im}\sum_{b,c}\left\{I_{da}^*(\omega_L)\left[|\mu_{ad}\mu_{dc}|^2 \times \frac{\bar{I}_{dc}(\omega_S)}{\omega_S - \omega_L - \omega_{ac} + i\Gamma_{ac}} + i(\Gamma^{-1})_{bb,dd}|\mu_{ad}\mu_{bc}|^2(\bar{I}_{bc}(\omega_S) - \bar{I}_{bc}^*(\omega_S))\right]\right\} \\ &= -2|\mu_{ad}|^2\,{\rm Im}\,I_{da}^*(\omega_L) \times \sum_{b,c}\left\{\left[\frac{|\mu_{dc}|^2 I_{dc}(\omega_S)}{\omega_S - \omega_L - \omega_{ac} + i\Gamma_{ac}} - 2|\mu_{bc}|^2(\Gamma^{-1})_{bb,dd}\,{\rm Im}[\bar{I}_{bc}(\omega_S)]\right]\right\}, \end{aligned} \quad \text{(A10)}$$

where we have introduced two complex line shape functions:

$$\begin{aligned} I_{\nu\lambda}(\omega) &= -i\int_0^\infty d\tau\, I_{\nu\lambda}(\tau)J_g(\tau)\exp(i\omega\tau) \\ &= (\omega + \Gamma_{\nu\lambda})^{-1} \end{aligned} \quad \text{(A11)}$$

and

$$\bar{I}_{\nu\lambda}(\omega) = -i\int_0^\infty d\tau\, I_{\nu\lambda}(\tau) J_b^{d*}(\tau)\exp(i\omega\tau). \quad \text{(A12)}$$

In the derivation of Eq. (A10) we further used the following identities:

$$I^*_{\nu\lambda}(\tau) = I_{\lambda\nu}(\tau) \quad \text{(A13a)}$$

and

$$-i\int_0^\infty d\tau\, I_{ac}(\tau)\exp(i\omega_S t - i\omega_L t) = (\omega_S - \omega_L - \omega_{ac} + i\Gamma_{ac})^{-1}. \quad \text{(A13b)}$$

In order to simplify Eq. (A10) further, we shall separate it into a Raman and a fluorescence components (denoted S_R and S_F, respectively). To that end we introduce the following assumptions. For the electronically excited state, the radiative rate γ_b^R is assumed to be independent on b, i.e.,

$$\gamma_b^R = \gamma^R. \quad \text{(A14a)}$$

We then get for the total decay rate of level $|b\rangle$,

$$\gamma_b = \gamma^R + \sum_{b'} \gamma_{b'b} = -\Gamma_{bb,bb}. \quad \text{(A14b)}$$

The decay rate of vibronic levels belonging to the ground electronic state is negligible, i.e.,

$$\gamma_a = \gamma_c = 0. \quad \text{(A15)}$$

We then get

$$\Gamma_{ac} = 1/2(\gamma_a + \gamma_c) = 0. \quad \text{(A16)}$$

Next, we split the $(\omega_S - \omega_L - \omega_{ac} + i\Gamma_{ac})^{-1}$ factor in Eq. (A10) into its real and imaginary parts,

$$(\omega_S - \omega_L - \omega_{ac} + i\Gamma_{ac})^{-1} = \mathrm{pp}(\omega_S - \omega_L - \omega_{ac})^{-1} - i\pi\delta(\omega_S - \omega_L - \omega_{ac}), \quad \text{(A17)}$$

where pp denotes the principal part. Substituting Eqs. (A14)–(A17) into Eq. (A10) allows us to split the emission rate $S_d(\omega_S)$ into Raman and fluorescence, i.e.,

$$S_d(\omega_S) = S_R(\omega_S) + S_F(\omega_S), \quad \text{(A18)}$$

where

$$S_R(\omega_S) = 2\pi\sum_c |\mu_{ad}\mu_{dc}|^2 I^*_{da}(\omega_L)\bar{I}_{bc}(\omega_S) \times\delta(\omega_S - \omega_L - \omega_{ac}) = 2\pi\sum_c |\mu_{ad}\mu_{dc}|^2 |I^*_{da}(\omega_L)|^2 \times\delta(\omega_S - \omega_L - \omega_{ac}) \quad \text{(A19)}$$

and

$$S_F(\omega_S) = -2\,\mathrm{Im}\sum_{b,c}\{I^*_{da}(\omega_L)[|\mu_{ad}\mu_{dc}|^2 \times\bar{I}_{dc}(\omega_S)\mathrm{pp}(\omega_S - \omega_L - \omega_{ac})^{-1} + 4|\mu_{ad}|^2\,\mathrm{Im}\, I^*_{da}(\omega_L)(\Gamma^{-1})_{bb,dd}|\mu_{bc}|^2 \times\mathrm{Im}[\bar{I}_{bc}(\omega_S)]]\}. \quad \text{(A20)}$$

The summation over b in the Eq. (A20) can be split into two parts: one is the summation over the redistributed states ($b \neq d$), and the other is the contribution of the doorway state $|d\rangle$. Since the emission from the doorway state does not involve any dephasing (the bath is at 0 K) the term $b = d$ in Eq. (A20) cancels.[6(a)] We then get

$$S_R(\omega_S) = 2\pi\sum_c \frac{|\mu_{ad}\mu_{dc}|^2}{(\omega_{ad} + \omega_L)^2 + (\gamma_d^2/4)} \times\delta(\omega_S - \omega_L - \omega_{ac}), \quad \text{(A21a)}$$

$$S_F(\omega_S) = \frac{2|\mu_{ad}|^2}{(\omega_{ad} + \omega_L)^2 + (\gamma_d^2/4)} \times\sum_{b\neq d}|\mu_{bc}|^2\gamma_b(\Gamma^{-1})_{bb,dd}\,\mathrm{Im}[\bar{I}_{bc}(\omega_S)]. \quad \text{(A21b)}$$

Combining Eqs. (A21a) and (A21b) results in

$$S_d(\omega_S) = \frac{2|\mu_{ad}|^2}{(\omega_{ad} + \omega_L)^2 + (\gamma_d^2/4)} \times\sum_{b,c}\{|\mu_{dc}|^2\delta(\omega_S - \omega_L - \omega_{ac}) + |\mu_{bc}|^2\gamma_b(\Gamma^{-1})_{bb,dd}\,\mathrm{Im}[\bar{I}_{bc}(\omega_S)]\}. \quad \text{(A22)}$$

When the definition of T [Eqs. (14)] is substituted in Eq. (A22) we obtain Eq. (13).

[1] See papers in *Photochemistry and Photobiology*, edited by A. H. Zewail (Harwood Academic, New York, 1983); Faraday. Discuss. Chem. Soc. **75** (1983).

[2] See papers in *Stochasticity and Intramolecular Redistribution of Vibrational Energy*, edited by R. Lefebvre and S. Mukamel (Reidel, New York, 1987).

[3] C. S. Parmenter, J. Phys. Chem. **86**, 1735 (1982); V. E. Bondybey, Annu. Rev. Phys. Chem. **35**, 591 (1984).

[4] S. Mukamel, J. Phys. Chem. **89**, 1077 (1985).

[5] P. H. Levy, Annu. Rev. Phys. Chem. **31**, 197 (1980); P. S. H. Fitch, L. Wharton, and D. H. Levy, J. Chem. Phys. **84**, 1099 (1986).

[6] (a) S. Mukamel and R. E. Smalley, J. Chem. Phys. **73**, 4156 (1980); (b) S. Mukamel, J. Chem. Phys. **82**, 2867 (1985).

[7] (a) A. Amirav, U. Even, and J. Jortner, J. Chem. Phys. **71**, 2319 (1979); (b) Chem. Phys. Lett. **72**, 17 (1980).

[8] T. Hayes, W. Henke, H. S. Selzle, and E. W. Schlag, Chem. Phys. Lett. **77**, 19 (1981).

[9] W. R. Lambert, P. M. Felker, and A. H. Zewail, J. Chem. Phys. **81**, 2195, 2209 (1984).

[10] (a) W. R. Lambert, P. M. Felker, and A. H. Zewail, J. Chem. Phys. **75**, 5958 (1981); (b) P. M. Felker, and A. H. Zewail, Chem. Phys. Lett. **102**, 113 (1983); (c) W. R. Lambert, P. M. Felker, and A. H. Zewail, J. Chem. Phys. **75**, 5958 (1981); (d) **81**, 2217 (1984); (e) P. M. Felker and A. H. Zewail, *ibid.* **82**, 2961, 2975 (1985).

[11] N. F. Scherer, J. W. Perry, F. E. Doany, and A. H. Zewail, J. Phys. Chem, **89**, 894 (1985); J. A. Syage, P. M. Felker, D. H. Semmes, F. Al Adel, and A. H. Zewail, J. Chem. Phys. **82**, 2896 (1985); P. M. Felker, W. R. Lambert, and A. H. Zewail, *ibid.* **82**, 3003 (1985); P. M. Felker and A. H. Zewail, Chem. Phys. Lett. **128**, 221 (1986).

[12] R. A. Coveleskie, D. A. Dolson, and C. S. Parmenter, J. Phys. Chem. **89**, 645 (1985); (b) **89**, 655 (1985); K. W. Holtzclaw and C. S. Parmenter, *ibid.* **88**, 3182 (1984); **84**, 1099 (1986); D. A. Dolson, K. W. Holtzclaw, D. B. Moss, and C. S. Parmenter, J. Chem. Phys. **84**, 1119 (1986).

[13] B. J. Berne and G. D. Harpe, Adv. Chem. Phys. **17**, 63 (1970).

[14] S. Mukamel, Phys. Rep. **93**, 1 (1982).

[15] R. G. Breene, *Theories of Spectral Lineshape* (Wiley, New York, 1981).

[16] G. R. Fleming, *Chemical Applications of Ultrafast Spectroscopy* (Oxford, London, 1986).

[17] See papers in *Proceedings of the Tenth International Conference on Ra-*

man Spectroscopy, edited by W. L. Peticolas and B. Hudson (University of Oregon, Eugene, 1986).
[18](a) S. Mukamel, S. Abe, Y. J. Yan and R. Islampour, J. Phys. Chem. **89**, 201 (1985); (b) Y. J. Yan and S. Mukamel, J. Chem. Phys. **85**, 5908 (1986); (c) Y. J. Yan and S. Mukamel, *ibid.* **86**, 6085 (1987).
[19]S. Mukamel, J. Chem. Phys. **71**, 2884 (1979); **82**, 5398 (1985); J. Sue, Y. J. Yan, and S. Mukamel, *ibid.* **85**, 462 (1986).
[20]S. Mukamel and R. F. Loring, J. Opt. Soc. Ann. B **3**, 595 (1986); R. F. Loring, Y. J. Yan, and S. Mukamel, Chem. Phys. Lett. **135**, 23 (1987); J. Phys. Chem. **91**, 1302 (1987).
[21]S. Mukamel, Adv. Chem. Phys. (in press).
[22]Y. R. Shen, *The Principles of Nonlinear Optics* (Wiley, New York, 1984).
[23]R. Zwanzig, Physica **30**, 1109 (1964).
[24]S. Mukamel, K. Shan, and Y. J. Yan, *Polycyclic Aromatic Hydrocarbons and Astrophysics*, edited by A. Leger, L. d'Hendercourt, and N. Boccara, NATO ASI Series, Vol. C 191, p. 129 (Reidel, Dordrecht, 1986).
[25]N. Van Kampen, *Stochastic Processes in Physics and Chemistry* (North Holland, Amsterdam, 1983).
[26]S. Mukamel and R. Islampour, Chem. Phys. Lett. **108**, 161 (1984).
[27]C. E. Porter, *Statistical Theories of Spectra: Fluctuations* (Academic, London, 1965).
[28]B. N. Cyvin and S. J. Cyvin, J. Phys. Chem. **73**, 1430 (1969), and references therein.
[29]D. J. Evans and D. B. Scully, Spectrochim. Acta **20**, 891 (1964), and references therein.
[30]G. M. Stewart, M. D. Ensminger, T. J. Kulp, R. S. Ruoff, and J. D. McDonald, J. Chem. Phys. **79**, 3190 (1983); G. M. Stewart, R. S. Ruoff, T. J. Kulp, and J. D. McDonald, *ibid.* **80**, 5353 (1984).